

# Remote weak signal measurement via bound states in optomechanical system

Xun Li,<sup>1,2</sup> Biao Xiong,<sup>1</sup> Shilei Chao,<sup>1</sup> Chengsong Zhao,<sup>1</sup> Hua-Tang Tan,<sup>3,\*</sup> and Ling Zhou<sup>1,†</sup>

<sup>1</sup>*School of Physics, Dalian University of technology, Dalian 116026, P.R.China*

<sup>2</sup>*National Key Laboratory of Shock Wave and Detonation Physics,  
Institute of Fluid Physics, China Academy of Engineering Physics, Mianyang 621900, China*

<sup>3</sup>*Department of Physics, Huazhong Normal University, Wuhan 430079, China*

## Abstract

A scheme for remote weak signal sensor is proposed in which a coupled resonator optical waveguide (CROW), as a transmitter, couples to a hybrid optomechanical cavity and an observing cavity, respectively. The non-Markovian theory is employed to study the weak force sensor by treating the CROW as a non-Markovian reservoir of the cavity fields, and the negative-effective-mass (NEM) oscillator is introduced to cancel the back-action noise. Under certain conditions, dissipationless bound states can be formed such that weak signal can be transferred in the CROW without dissipation. Our results show that ultrahigh sensitivity can be achieved with the assistance of the bound states under certain parameters regime.

**Keywords:** cavity optomechanics, remote detection, non-Markovian environment, quantum noise

---

\* tht@mail.ccnu.edu.cn

† zhllxn@dlut.edu.cn

## I. INTRODUCTION

Optomechanical system, involving the coupling between mechanical motion and cavity field, provides us a high sensitive device to detect weak force, tiny mass and displacement of the mechanical motion [1, 2]. With the advance of micro-nano technology, micro-cavity optomechanical systems with high mechanical frequency, high quality factor and strong optomechanical coupling are realized in several kinds of systems such as whispering-gallery-mode resonator [3–7], levitated nano-sphere [8, 9] and optomechanical crystal [10, 11]. These progresses push optomechanical systems in the precision detection further into application. Approaches to force detection [12, 13] based on nano-mechanical systems are well-established and have been used for measuring displacement [14]. Increasingly, it is believed that next-generation mechanical biosensor may be realized in nano-mechanical systems, because they are particularly matched in size with molecular interactions, and provide a basis for biological probes with single-molecule sensitivity [15, 16]. For the biosensing and medical diagnoses or other detection scenario, the local detection scheme might not meet the needs of practical demand, it is necessary to construct waveguide-optomechanical coupling system so as to perform remote detection. To our knowledge, this remote force detection has not yet been investigated.

The sensitivity of optomechanical detector is limited by the noise. Various proposals have been put forward for reducing noise, including squeezing of mechanical oscillator [17–20] frequency-dependent squeezing of optical field [21–23], two-tone measurements, dual mechanical oscillator configurations [24, 25], and atomic assistance detection [26–28]. Especially, it has been shown that quantum back-action (QBA) noise can be cancelled when the prob field couples to positive and negative-effective-mass (NEM) oscillators simultaneously [26, 29, 30]. The QBA free proposal has been realized in a hybrid cavity optomechanical system in which a spin ensemble plays the role of the negative-mass oscillator [31].

For remote detection, the waveguide is usually employed to connect the sensor and the detector. Using tapered fibers coupling to sensing cavity has been investigated in [14, 32]. In the purpose of integrating the system on chip and improving the detection precision, the waveguide integrated in the sensing cavity has been realized in microcavity regime [33, 34]. Theoretically, the waveguide can be treated as structured reservoirs [35–39], and the theory of non-Markovian quantum open system is an effective method to study the dynamics

of the objects coupling to the reservoir. In cavity quantum electrodynamics regime, the structured reservoir can be photonic crystals or waveguides [37, 40–44]. It has been shown that the bound states without dissipation can be formed when system coupled to band gaps or finite band spectrum [36, 45] which is easily satisfied in photonic crystals or waveguides [35, 36, 41, 46, 47]. The dissipationless of bound state benefits the transfer of the signals.

Since the QBA evading in hybrid optomechanical system had been realized in experiment [31], in the paper, we put forward a proposal by generating QBA evading measurement to remote force detection. Using non-Markovian theory, we solve the dynamics and obtain the output signal of the hybrid system. We carefully investigate the surviving condition of the bound state and show that the output fields can be transferred in the presence of bound state. A high precision and minimized weak force sensor can be achieved. Different from the researches [12, 13, 48], we consider a remote weak force detection, which may be more suitable in some cases. In order to avoid the photon consumption of the waveguide, we investigated the condition of the bound state, which should be meaningful for experimental realization.

This paper is arranged as follows. In Sec. II, we present the model and Hamiltonian of our proposal. We study the effective non-Markovian reservoir and the bound states in Sec. III. The sensitivity and the mechanism of suppressing the noise are discussed in Sec. IV. Finally, Sec. V gives a summary of this work.

## II. MODEL AND HAMILTONIAN

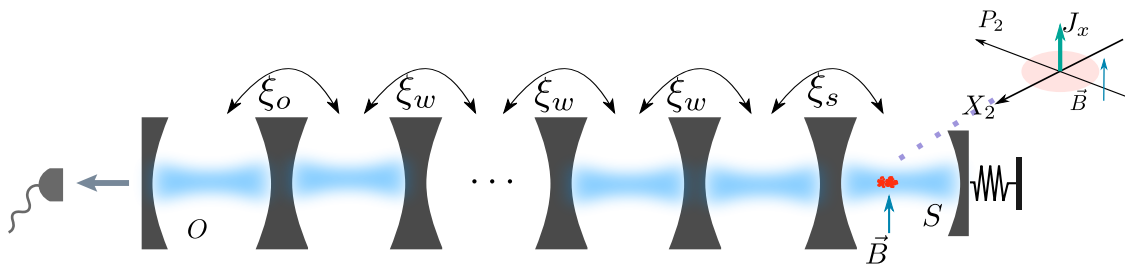


FIG. 1. The sketch of hybrid optomechanical system where a waveguide couples to the optomechanical cavity  $S$  and an observing cavity  $O$ . The atomic ensemble in a static magnetic field with specific direction can be regarded as a NEM spin oscillator (detail structure see [31]).

In order to detect remote weak signal, we employ a hybrid cavity optomechanical system, shown in Fig. 1. In the cavity  $S$ , the movable mirror works as a sensor, and the fixed mirror of the cavity  $S$  is connected to a CROW so that the signal can be transmitted to the observing cavity  $O$  and be read out by homodyne detector. In addition, an atomic ensemble whose spin direction  $\vec{\mathbf{J}}$  can be manipulated by a magnetic field  $\vec{\mathbf{B}}$  is placed in cavity  $S$ . Employing the same procedure as in [26, 31], the spin of the atomic ensemble can be effectively equivalent to an oscillator with effective-negative-mass; therefore, the noise of quantum back-action can be evaded. The Hamiltonian of the system can be written as

$$H = H_{OM} + H_{\text{crow}}, \quad (1)$$

with

$$H_{OM} = \frac{p_1^2 - p_2^2}{2m} + \frac{m}{2}\omega_m^2(q_1^2 - q_2^2) + \hbar g a_s^\dagger a_s (q_1 + q_2) + \hbar \omega_s a_s^\dagger a_s + f q_1. \quad (2)$$

The first and the second terms express the Hamiltonian of the mechanical oscillator and the NEM oscillator (the detailed description of the atom ensemble equivalence to NEM oscillator can be referred in [31]) where  $q_1$  ( $p_1$ ) is the position (momentum) operator of the mechanical oscillator,  $q_2$  ( $p_2$ ) is the position (momentum) operator of NEM oscillator. To cancel the back-action noise, we let the two oscillators have the same mass ( $m$ ) and frequencies ( $\omega_m$ ) as had reported by Ref. [31]. The third term describe the coupling between the two oscillators and the cavity  $S$  where the NEM oscillator couples to the field with the same form as the optomechanical interaction [49].  $a_s$  ( $a_s^\dagger$ ) is the creation (annihilation) operator of the sensing cavity  $S$ , and  $g$  is the coupling strength. The fourth term is the energy of the cavity  $S$ , and the last term describes the weak force  $f$  coupling to the mechanical oscillator.

When defining collective position  $Q = (q_1 + q_2)$  and collective momentum  $P = \frac{1}{2}(p_1 + p_2)$ , relative position  $\Phi = \frac{1}{2}(q_1 - q_2)$  and relative momentum  $\Pi = p_1 - p_2$ , the Hamiltonian can be transformed into

$$H_{OM} = \frac{P\Pi}{m} + m\omega_m^2 Q\Phi + \hbar g a_s^\dagger a_s Q + f(Q + 2\Phi) + \hbar \omega_s a_s^\dagger a_s. \quad (3)$$

We have the commutation  $[Q, \Pi] = 0$  and  $[P, \Phi] = 0$ . Therefore, the collective position  $Q$  (momentum  $P$ ) and relative momentum  $\Pi$  (position  $\Phi$ ) are a pair of observable operators which can be simultaneously measured with arbitrary precision.

As shown in Fig. 1, the CROW consists of  $N$ -cavity chain, and the CROW couple to the optomechanical sensing cavity  $S$  and observing cavity  $O$ , respectively. The Hamiltonian of the CROW can be written as

$$H_{\text{crow}} = \sum_{n=1}^N \hbar\omega_w a_n^\dagger a_n - \sum_{n=1}^{N-1} \hbar\xi_w (a_n^\dagger a_{n+1} + a_{n+1}^\dagger a_n) + \hbar\xi_s (a_1^\dagger a_s + a_s^\dagger a_1) + \hbar\xi_o (a_N^\dagger a_o + a_o^\dagger a_N) + \hbar\omega_o a_o^\dagger a_o + i\hbar E_o (a_o^\dagger e^{-i\omega_d t} - a_o e^{i\omega_d t}), \quad (4)$$

where the first term is the energy of CROW, the second term stands for the hopping between the nearest neighbor cavity with rate  $\xi_w$ , the third and the fourth terms describe the coupling of the cavity  $S$  and the cavity  $O$  to the 1st and  $N$ th cavity of CROW respectively, where  $a_o$  ( $a_o^\dagger$ ) is the annihilation and creation operator of cavity  $O$ , the fifth term is the energy of cavity  $O$ , the last term represents the classical driven of cavity  $O$  with frequency  $\omega_d$  and strength  $E_o$ . Performing the Fourier transformation [41]

$$a_k = \sqrt{\frac{2}{\pi}} \sum_{n=1}^N \sin(nk) a_n \quad (0 < k < \pi), \quad (5)$$

then we can rewrite the Hamiltonian  $H_{\text{crow}}$  as

$$H_{\text{crow}}/\hbar = \omega_o a_o^\dagger a_o + \sum_k \omega_k a_k^\dagger a_k + \sum_{j=s,o} \sum_k V_j(k) (a_j^\dagger a_k + a_k^\dagger a_j) + iE_o (a_o^\dagger e^{-i\omega_d t} - a_o e^{i\omega_d t}), \quad (6)$$

where  $\omega_k = \omega_w - 2\xi_w \cos k$ ,  $V_j(k) = \xi_j \sqrt{\frac{2}{\pi}} \sin(n_j k)$  ( $n_s = 1, n_o = N$ ). The Hamiltonian Eq. (6) implies that the CROW can be regarded as a structured reservoir of the cavity  $S$  ( $O$ ). In order to exactly solve the dynamics of the system, the non-Markovian treatment should be employed. The coupled cavity chain or waveguide is equivalent to a structured reservoir has been investigated in [41]. Here, we employ the coupled cavity chain to transmit information of weak signal from the sensor to the detector. For simplicity, we assume that the CROW is ideal without coupling to additional environment.

After switching into a frame rotating with respect to  $H_0 = \hbar\omega_d (a_o^\dagger a_o + a_s^\dagger a_s + \sum_k a_k^\dagger a_k)$ , and nondimensionalizing operators with transform:  $g \rightarrow g\sqrt{m\omega_m/\hbar}$ ,  $f \rightarrow f\sqrt{\hbar\omega_m m}$ ,  $Q \rightarrow Q\sqrt{\hbar/m\omega_m}$ ,  $\Phi \rightarrow \Phi\sqrt{\hbar/\omega_m m}$ ,  $P \rightarrow P\sqrt{\hbar\omega_m m}$  and  $\Pi \rightarrow \Pi\sqrt{\hbar\omega_m m}$ , the Hamiltonian can be changed into time-independent form as

$$H/\hbar = \omega_m (P\Pi + Q\Phi) + g a_s^\dagger a_s Q + f (Q + 2\Phi) + \Delta_s a_s^\dagger a_s + \Delta_o a_o^\dagger a_o + iE_o (a_o^\dagger - a_o) + \sum_k \Delta_k a_k^\dagger a_k + \sum_{j=s,o} \sum_k V_j(k) (a_j^\dagger a_k + a_k^\dagger a_j), \quad (7)$$

where  $\Delta_j = \omega_j - \omega_d$  ( $j = s, o, k$ ). We will use Eq. (7) to calculate the output of the weak signal (weak force  $f$ ).

### III. THE EFFECTIVE NON-MARKOVIAN RESERVOIR AND THE BOUND STATES

As we have pointed out that the coupled cavity chain is equivalent to a structured reservoir, we now need to solve the dynamics with non-Markovian theory.

Using the Hamiltonian Eq. (7), we can obtain the Heisenberg equations as

$$\dot{Q} = \omega_m \Pi, \quad (8a)$$

$$\dot{\Pi} = -\omega_m Q - 2f - \frac{\gamma_m}{2} \Pi + \sqrt{\gamma_m} \Pi^{\text{in}}, \quad (8b)$$

$$\dot{a}_s = -i\Delta_s a_s - \frac{\kappa_s}{2} a_s - i g a_s Q - i \sum_k V_s a_k + \sqrt{\kappa_s} a_s^{\text{in}}, \quad (8c)$$

$$\dot{a}_o = -i\Delta_o a_o - \frac{\kappa_o}{2} a_o - i \sum_k V_o a_k + E_o + \sqrt{\kappa_o} a_o^{\text{in}}, \quad (8d)$$

$$\dot{a}_k = -i\Delta_k a_k - i \sum_{j=s,o} V_j a_j, \quad (8e)$$

where  $\kappa_j$  and  $a_j^{\text{in}}$  ( $j = s, o$ ) are the damping rate and noise operator of the cavities  $S$  and  $O$ , the negative and positive oscillators have same damping  $\gamma_m$ , and  $\Pi^{\text{in}} = p_1^{\text{in}} - p_2^{\text{in}}$  is thermal noise of the oscillator, in which  $p_1^{\text{in}}$  ( $p_2^{\text{in}}$ ) is noise operator of normal (NEM) oscillator, and the correlation function has the relation  $\langle p_1^{\text{in}} p_2^{\text{in}} \rangle = 0$ , then  $\langle \Pi^{\text{in}}(t) \Pi^{\text{in}}(t') \rangle = 2 \coth\left(\frac{\hbar \omega_m}{2 k_B T}\right) \delta(t - t')$ . From Eqs. (8a) and (8b), it is obvious that the collective position  $Q$  and relative momentum  $\Pi$  form a QBA free system. Due to  $[Q, \Pi] = 0$ , the collective position  $Q$  and relative momentum  $\Pi$  can be simultaneously measured with arbitrary precision. The variance of  $Q$  ( $\Pi$ ) does not affect the variance of  $\Pi$  ( $Q$ ) although the  $\Pi$  is related with  $Q$  (see Eq. (8b)). Since the cavity  $S$  ( $O$ ) works as a sensor (detector), the dissipation should be included because it is an open system in order to sense (output) signal, while the cavity chain functions as a transmitter, and it is reasonable to ignore the loss of the chain for high quality cavities.

Through integrating Eq. (8e), the formal solution of  $a_k(t)$  can be obtained

$$a_k(t) = a_k(0) e^{-i\Delta_k t} - i \int_0^t d\tau e^{-i\Delta_k(t-\tau)} \sum_{j=s,o} V_j a_j(\tau). \quad (9)$$

Inserting Eq. (9) into Eqs. (8c) and (8d), we obtain

$$\dot{a}_s = -i(\Delta_s - i\frac{\kappa_s}{2})a_s - iga_s Q + A_s^{\text{in}} - \int_0^t d\tau \int d\omega \sum_{j=s,o} J_{sj}(\omega) a_j(\tau) e^{-i\omega(t-\tau)}, \quad (10)$$

$$\dot{a}_o = -i(\Delta_o - i\frac{\kappa_o}{2})a_o + E_o + A_o^{\text{in}} - \int_0^t d\tau \int d\omega \sum_{j=s,o} J_{oj}(\omega) a_j(\tau) e^{-i\omega(t-\tau)}, \quad (11)$$

where  $A_j^{\text{in}} = \tilde{a}_j^{\text{in}} + \sqrt{\kappa_j} a_j^{\text{in}}$  is the noise operator, and  $\tilde{a}_j^{\text{in}} = -i \sum_k V_j a_k(0) e^{-i\Delta_k t}$  is the noise operator of the structured reservoir. With the transform  $\sum_k \rightarrow \int d\omega dk/d\omega = \int d\omega \varrho(\omega)$  [41] in which  $\omega$  means relative frequency  $\Delta_k = \omega_k - \omega_d$ , that is  $\omega = \Delta_w - 2\xi_w \cos(k)$  with  $\Delta_w = \omega_w - \omega_d$ , we can obtain the spectrum function as

$$J_{ij}(\omega) = \varrho(\omega) V_i^*(\omega) V_j(\omega), \quad (12)$$

where

$$\varrho(\omega) = \frac{1}{\sqrt{(2\xi_w)^2 - (\Delta_w - \omega)^2}}, \quad (13)$$

and

$$V_i(\omega) = \sqrt{\frac{2}{\pi}} \xi_i \sin \left[ n_i \arcsin \left( \sqrt{1 - \left( \frac{\omega - \Delta_w}{2\xi_w} \right)^2} \right) \right]. \quad (14)$$

Considering the sensing cavity pumping with classical field, we can expand the cavity field as  $a_j \rightarrow \alpha_j + a_j$  ( $j = s, o$ ), which means that the cavity field can be decomposed to the classical mean value  $\alpha_j$  plus its quantum part, so that the dynamical equation can be linearized. In strong non-Markovian regime,  $\alpha_j$  does not mean the steady-state values of the cavity field  $a_j$ . From Eqs. (8a) and (8b), it is easy to verify that  $\langle Q \rangle$  is independent of the cavity fields due to the interference between the two oscillator, which indicates that the self-sustained oscillation of optomechanical system which is an obstacle of linearization is suppressed. The situation is different from the generic optomechanical system [48, 50] where the zero point of the mechanical oscillator is displaced due to the radiation pressure. According to Eq. (10) and (11), we have

$$\dot{\boldsymbol{\alpha}} = -i\tilde{\boldsymbol{\Delta}} \cdot \boldsymbol{\alpha} - \mathbf{E} + \int_0^t d\tau \int d\omega \mathbf{J}(\omega) \cdot \boldsymbol{\alpha}(\tau) e^{-i\omega(t-\tau)}, \quad (15)$$

where

$$\mathbf{J}(\omega) = \begin{bmatrix} J_{so}(\omega) & J_{ss}(\omega) \\ J_{oo}(\omega) & J_{os}(\omega) \end{bmatrix}, \quad (16)$$

$\boldsymbol{\alpha}(t) = [\alpha_s(t), \alpha_o(t)]^T$ ,  $\tilde{\boldsymbol{\Delta}} = \text{diag}[\tilde{\Delta}_s, \tilde{\Delta}_o]$  with  $\tilde{\Delta}_s = \Delta_s - i\frac{\kappa_s}{2} + g\langle Q \rangle$ ,  $\tilde{\Delta}_o = \Delta_o - i\frac{\kappa_o}{2}$  and  $\mathbf{E} = [0, E_o]^T$ . We perform the Laplace transformation  $O(z) = \int_0^\infty dt O(t) e^{izt}$  to solve the dynamic evolution  $\alpha_j$ , with initial values  $\boldsymbol{\alpha}(0) = 0$ , we can obtain

$$z\boldsymbol{\alpha}(z) = \tilde{\boldsymbol{\Delta}} \cdot \boldsymbol{\alpha}(z) - \frac{1}{z}\mathbf{E} + \boldsymbol{\sigma}(z) \cdot \boldsymbol{\alpha}(z), \quad (17)$$

where  $\boldsymbol{\sigma}(z) = \int d\omega \frac{\mathbf{J}(\omega)}{z-\omega}$  is the self-energy matrix. In order to obtain a simple and clear meaning of the solution of above equation, we first assume  $E_o$  absence to obtain a Green's function  $\bar{\alpha}_j(\tau)$ . Then, we have

$$\bar{\alpha}_s(z) = i \frac{\sigma_{so}}{\mathcal{D}(z)}, \quad (18)$$

where

$$\mathcal{D}(z) = [z - \tilde{\Delta}_s - \sigma_{ss}(z)][z - \tilde{\Delta}_o - \sigma_{oo}(z)] - \sigma_{so}(z)\sigma_{os}(z), \quad (19)$$

and for more details seeing Appendix A. With the relation  $\alpha_j(t) = E_o \int_0^t d\tau \bar{\alpha}_j(\tau)$  and the inverse Laplace transform, we obtain the solution in the long-time limit

$$\alpha_s(t \rightarrow \infty) = \sum_{n'=1}^{N_b} \frac{iE_o}{\omega_{r_{n'}}} \mathcal{Z}_{n'} e^{-i\omega_{r_{n'}}t} - E_o \sum_{n=1}^{N_p} \frac{i\mathcal{Z}_n}{\omega_{r_n}} + I_{NE}, \quad (20)$$

where  $N_b$  is the number of poles on the first Riemannian sheet, and  $N_p$  is the number of poles on the first and second Riemannian sheet. We can find all the poles of  $\bar{\alpha}_s(z)$  denoted as  $\omega_{r_n}$  through solving  $\mathcal{D}(z) = 0$ . The poles are classical by its position. It can be proof that when the poles on first Riemannian sheet where  $\text{Re}(\omega_{r_n}) < \Delta_w - 2\xi_w$  or  $\text{Re}(\omega_{r_n}) > \Delta_w + 2\xi_w$  the poles must be on the real axis. (for more details seeing Appendix A and B). We denote this pole as  $\omega_{r_{n'}}$  which is real number, the first term in Eq. (20) will be exponent oscillation term without dissipation, and this state is called bound state.  $\mathcal{Z}_{n'}$  is the residues of at poles  $\omega_{r_{n'}}$ . All the poles on the first and second Riemannian sheet with residues  $\mathcal{Z}_n$  contribute to the second terms. The last term is non-exponential decay, and it is studied in Appendix C.

Since the cavity chain is equivalent to a reservoir, the reservoir will induce dissipation for the cavity  $S$  and  $O$ . In order to transmit weak signal, we expect that the cavity chain can transfer the signal without dissipation. Fortunately, the bound state is exponent oscillator without dissipation and can fulfil the task. In other word, bound state is important and play the special role in the remote weak signal detection. We now discuss the parameter region in which the bound state exists.



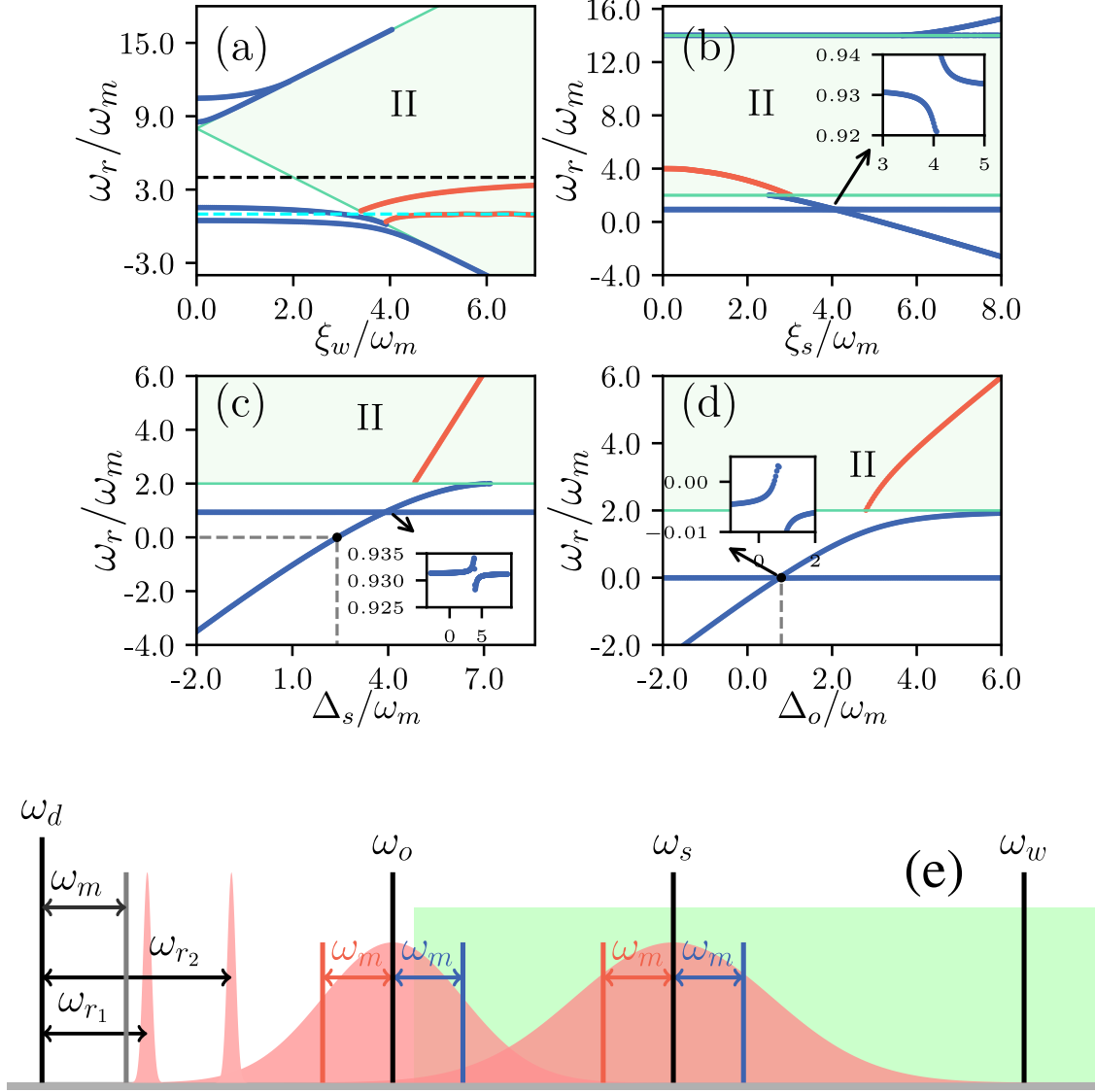


FIG. 2. The frequency  $\omega_r$  as the function of  $\xi_w$  (a),  $\xi_s$  (b),  $\Delta_s$  (c) and  $\Delta_o$  (d); the blue curves stand for the bound states, while the red curves for the poles leading to exponential decay. The black and cyan dashed lines in (a) represent  $\Delta_s$  and  $\Delta_o$ , respectively. The inset of (b), (c) and (d) for zoom-in of the cross point. (e) The diagram of cavity mode and its sideband in optomechanical system, where the red peaks with large width labeled as  $\omega_o$  and  $\omega_s$  represent the bare cavity modes, and the green area corresponds to  $\Delta_w - 2\xi_w < \omega < \Delta_w + 2\xi_w$  (without bound states). The frequencies of bound states are adjustable. The parameters which are unspecified before, are  $\Delta_w = 8\omega_m$ ,  $\Delta_s = 4\omega_m$ ,  $\Delta_o = 2\omega_m$ ,  $\xi_w = 3\omega_m$ ,  $\xi_s = 4\omega_m$ ,  $\xi_o = 2\omega_m$ ,  $E_o = 2 \times 10^5 \omega_m$ ,  $\kappa_s = 0.01\omega_m$ ,  $\kappa_o = 0.05\omega_m$ ,  $g = 0.002\omega_m$ , and  $N = 30$ .

We numerically calculate the poles of  $\bar{\alpha}_s(z)$  and plot the real part of pole vs several parameters shown in Fig. 2. In the green area, the condition  $\Delta_w - 2\xi_w < \omega_r < \Delta_w + 2\xi_w$  (determined by making positivity of the radicand of Eq. (13)) is satisfied, which stands for the second Riemannian sheet. Beyond the green area, we call it first Riemannian sheet. As it is shown in Fig. 5 in the Appendix A, the poles on the first Riemannian sheet can keep the oscillation well, while the poles on the second Riemannian sheet can turn the oscillation into exponential decay because of the large imaginary part. Therefore, the poles in the first Riemannian sheet is superior than the ones in the second Riemannian sheet in against dissipation.

The blue curves in the Fig. 2(a) represent the poles on the first Riemannian sheet, while the red ones represent the poles on the second sheet. With the increasing of  $\xi_w$ , the blue curves converge to the border of the light-green area, or vanish, which means that small value of  $\xi_w$  is favor of surviving of bound states. As we can see from Eq. (12),  $\xi_w$  determines the width of spectrum, the larger  $\xi_w$ , the weaker non-Markovianity. This phenomenon reflects that with a large width of spectrum the system converge to a Markovian system where poles converge to  $\Delta_s$  and  $\Delta_o$ . In other word, strong non-Markovianity does not need strong nearest-neighbor coupling of cavities.

In Fig. 2(b), we study the poles as the function of  $\xi_s$ . When  $\xi_s$  is small, we can obtain two poles with the same value of  $\xi_s$ , but only one pole is in the first Riemannian sheet, and the other poles is in the second Riemannian sheet. With the increasing of the value of  $\xi_s$ , the two poles are both in first Riemannian sheet, and a high-frequency bound state is generated. Therefore, small  $\xi_w$  and large  $\xi_s$  are benefit to obtain the bound states. In addition, one of the poles almost is not affected by the value of  $\xi_s$ , only the other pole strongly depend on the value of  $\xi_s$ , which means that the bound states are mainly determined by the coupling between the cavity  $S$  ( $O$ ) and the common environment, respectively. However, it is interesting to find from the inset in Fig. 2(b) that the frequencies of bound states sharply change when the two bound states have very close frequencies. In this case, small disturbance can make a jump between the two bound states.

In Fig. 2(c) and (d), we study the poles as the function of  $\Delta_s$  and  $\Delta_o$ . In Fig. 2(c), we find that a bound state will disappear when  $\Delta_s \approx 7\omega_m$ , and poles in second Riemannian sheet will appear when  $\Delta_s$  is increasing to  $\Delta_s \approx 4\omega_m$ . To generate bound states, the frequency of cavity field should keep away from the center frequency of CROW ( $\Delta_w = 8\omega_m$ ). The same

result can be obtained for  $\Delta_o$ . The ‘‘cross point’’ in Fig. 2(c) and (d) are similar with the one in Fig. 2(b) where frequencies of bound states sharply change with the parameters. In addition, we would like to mention the special points in (c) and (d) because we will use the special points in Fig. 3. See Fig. 2(c), when  $\Delta_s = 2.4\omega_m$ , the frequencies of the two bound states are  $\omega_{r_1} \approx 0$  and  $\omega_{r_2} \approx \omega_m$ . In Fig. 2(d), when  $\Delta_s = 2.4\omega_m$ , and  $\Delta_o = 0.8\omega_m$ , we have  $\omega_{r_1} \approx \omega_{r_2} \approx 0$ .

In the plotting Figs. 2(a) to (d), the optomechanical interaction is ignored because it only appears in  $\tilde{\Delta}_s = \Delta_s - i\frac{\kappa_s}{2} + g\langle Q \rangle$ , and the displacement resulted from radiation pressure is extremely small, compared with  $\Delta_s - i\frac{\kappa_s}{2}$ , so here we choose  $\langle Q \rangle = 0$  [31]. Therefore, the bound states actually are formed by the three-body interaction among the cavity S, O and the CROW. In order to make the frequencies of bound state matching the frequency of the sensing oscillator, we choose the parameters of Fig. 2 in the unit of  $\omega_m$  and summarize the relation of the several frequencies of the fields in Fig. 2(e). Since the cavity S (O) couple to a common reservoir CROW, the effective decay rates of cavity S (O) are enhanced by the coupling strength  $\xi_s$  ( $\xi_o$ ), which is represented by the two red peaks with large width. Fortunately, the bound states is free of this problem. When the bound states couple to mechanical oscillator, we can select special bound states, for instance, when  $\omega_{r_1} \approx \omega_{r_2} \approx \omega_m$ , the sidebands are coincident; when  $\omega_{r_1} \approx 0$  and  $\omega_{r_2} \approx \omega_m$ , one bound state resonates with driven field, and the other resonates with oscillator; when  $\omega_{r_1} \approx \omega_{r_2} \approx 0$ , two bound states resonates with driven field. We will show that in this way the output signal can be enhanced.

#### IV. THE SENSITIVITY OF WEAK SIGNAL

We now study the sensitivity of weak signal detection. As we have pointed out that the bound state means the long-life oscillation, it benefits the transmission of the signal. Under this condition, the coupling between the mechanical oscillator and the cavity mode  $a_s$  is of the form  $G = \alpha_s g = G_0 + \sum_{n=1}^{N_b} G_n e^{-i\omega_{r_n} t}$  where  $G_n = -igE_o \mathcal{Z}_n / \omega_{r_n}$  corresponds to bound states  $\omega_{r_n}$  and  $G_0 = g(I_{NE} - E_0 \sum_{n=1}^{N_p} \frac{i\mathcal{Z}_n}{\omega_{r_n}})$ . The Heisenberg-Langevin equations after linearized can be obtained as

$$\dot{a}_s = -i\tilde{\Delta}_s a_s - iGQ + A_s^{\text{in}} - \int_0^t d\tau \int d\omega \sum_{j=s,o} J_{sj}(\omega) a_j(\tau) e^{-i\omega(t-\tau)}, \quad (21a)$$

$$\dot{a}_o = -i\tilde{\Delta}_o a_o + A_o^{\text{in}} - \int_0^t d\tau \int d\omega \sum_{j=s,o} J_{oj}(\omega) a_j(\tau) e^{-i\omega(t-\tau)}, \quad (21b)$$

$$\dot{Q} = \omega_m \Pi, \quad (21c)$$

$$\dot{\Pi} = -\omega_m Q - 2f - \frac{\gamma_m}{2} \Pi + \sqrt{\gamma_m} \Pi^{\text{in}}. \quad (21d)$$

Without back-action evading technique, the back-action force  $Ga_s^\dagger + G^*a_s$  will act on Eq. (21d) [48], and it adds a noise channel. The above equations can be changed into frequency domain

$$\omega a_s(\omega) = \tilde{\Delta}_s a_s(\omega) + \mathcal{L}[GQ] + \sum_{j=s,o} \sigma_{sj} a_j(\omega) + iA_s^{\text{in}}(\omega), \quad (22a)$$

$$\omega a_o(\omega) = \tilde{\Delta}_o a_o(\omega) + \sum_{j=s,o} \sigma_{oj} a_j(\omega) + iA_o^{\text{in}}(\omega), \quad (22b)$$

$$-i\omega Q(\omega) = \omega_m \Pi(\omega), \quad (22c)$$

$$-i\omega \Pi(\omega) = -\omega_m Q(\omega) - 2f(\omega) - \frac{\gamma_m}{2} \Pi(\omega) + \sqrt{\gamma_m} \Pi^{\text{in}}(\omega). \quad (22d)$$

We let  $\mathcal{L}[GQ] = \sum_{n=0}^{N_b} G_n Q(\omega - \omega_{r_n})$ , by setting  $\omega_{r_0} = 0$  ( $\omega_{r_0}$  is a denotation not a bound state). According to Eq. (22a) and (22d), we obtain

$$Q(\omega) = \chi_m(\omega) [2f(\omega) - \sqrt{\gamma_m} \Pi^{\text{in}}(\omega)], \quad (23)$$

where  $\chi_m(\omega) = \omega_m(\omega^2 - \omega_m^2 + \frac{i}{2}\gamma_m\omega)^{-1}$  is the response function. The solution of  $a_o$  in frequency domain can be obtained as

$$a_o(\omega) = i\bar{\alpha}_o(\omega) A_o^{\text{in}}(\omega) + \bar{\alpha}_s(\omega) \left[ \sum_{n=0}^{N_b} G_n Q(\omega - \omega_{r_n}) + iA_s^{\text{in}}(\omega) \right], \quad (24)$$

in which  $\bar{\alpha}_j(\omega)$  ( $j = s, o$ ) is Green function  $\bar{\alpha}_j(t)$  in frequency domain, where  $\bar{\alpha}_j$  is given in Eq. (A2). The output of the observing cavity is given by  $a_o^{\text{out}} = a_o^{\text{in}} - \sqrt{\kappa_o} a_o$ . According to Eq. (24), the status of the oscillator is monitored by the cavity field. Therefore, the weak signal can be read out through homodyne detection by measuring the quadrature [2]

$$M = a_o^{\text{out}} e^{-i\theta} + a_o^{\text{out}\dagger} e^{i\theta} \quad (25)$$

where  $\theta$  is an adjustable phase. In the frequency domain, the relation between signal and the quadrature can be obtained

$$M(\omega) = \sqrt{\kappa_o} e^{-i\theta} \left\{ \frac{a_o^{\text{in}}(\omega)}{\sqrt{\kappa_o}} - i\bar{\alpha}_o(\omega) A_o^{\text{in}}(\omega) + i\bar{\alpha}_s(\omega) A_s^{\text{in}}(\omega) + \bar{\alpha}_s(\omega) \left[ \sum_{n=0}^{N_b} G_n \chi_m(\omega - \omega_{r_n}) \left( 2f(\omega - \omega_{r_n}) - \sqrt{\gamma_m} \Pi^{\text{in}}(\omega) \right) \right] \right\} + H.c.. \quad (26)$$

From above equation, we can see that the response function  $\chi_m$  and  $\bar{\alpha}_o$  joint together to response the weak signal. If both of them achieve their maximum values, then we can achieve the optimized response. It is why we discuss the bound state in Fig. 2. In addition, due to the introducing of a NEM oscillator, the back-action noise of the cavity  $S$  is eliminated, only the thermal noise of  $\Pi^{\text{in}}$  exists, which is different from our early work [48] where the additional noise contains the back-action noise proportional to the optomechanical coupling  $G$ . We would like to amplify the signal  $f$  while the noise can be suppressed as low as possible. Therefore, the level of the noise is very important in the weak signal detection. We employ the definition of noise force (additional force) [26] as

$$F_{\text{add}}(\omega) = \left. \frac{M(\omega)}{\partial M(\omega)/\partial f} \right|_{f=0}. \quad (27)$$

According Eq. (26), the addition force can be obtained as

$$F_{\text{add}}(\omega) = F_o(\omega) - \frac{\sqrt{\gamma_m}}{2} \Pi^{\text{in}}(\omega), \quad (28)$$

where

$$F_o(\omega) = \frac{\mathcal{A}(\omega)e^{-i\theta}}{\sqrt{\kappa_o}} \left\{ a_o^{\text{in}}(\omega) + i\sqrt{\kappa_o}[-\bar{\alpha}_o(\omega)A_o^{\text{in}}(\omega) + \bar{\alpha}_s(\omega)A_s^{\text{in}}(\omega)] \right\} + H.c. \quad (29)$$

is noise induced by the cavity fields in which

$$\mathcal{A}(\omega) = \left[ 2 \sum_{n=0}^{N_b} e^{-i\theta} \bar{\alpha}_s(\omega) G_n \chi_m(\omega - \omega_{r_n}) + H.c. \right]^{-1}. \quad (30)$$

The noise spectrum can defined as

$$S_{\text{add}}(\omega) = \frac{1}{2} \int d\omega' \left\langle F_{\text{add}}(\omega) F_{\text{add}}(\omega') + (\omega \leftrightarrow \omega') \right\rangle. \quad (31)$$

If the signal is more weak than the noise, it definitely can not be detected from the background noise. Therefore, the noise level determines the accuracy of the weak signal detection. So, it is reasonable to define the force sensitivity using

$$F_s(\omega) = \sqrt{\hbar m \omega_m S_{\text{add}}(\omega)}, \quad (32)$$

where  $\hbar m \omega_m$  is introduced to recover the units because we have nondimensionalized the Hamiltonian basing on  $\omega_m$  and  $\hbar$  [51]. The thermal noise operator  $\Pi^{\text{in}}$  is the incoherent superposition of the thermal noise of the positive and negative oscillators. Considering

the same frequency and damping rate of positive and negative oscillators, the correlation function in frequency domain can be obtained as

$$\langle \Pi^{\text{in}}(\omega') \Pi^{\text{in}}(\omega) \rangle = 2 \coth\left(\frac{\hbar\omega_m}{2k_B T}\right) \delta(\omega + \omega'), \quad (33)$$

where  $T$  is temperature and  $k_B$  is the Boltzmann constant [52]. The noise operator of cavity fields consist of two parts whose correlation functions are

$$\langle a_i^{\text{in}}(\omega) a_j^{\text{in}\dagger}(\omega') \rangle = \delta_{ij} \delta(\omega + \omega'), \quad (34)$$

and

$$\langle \tilde{a}_i^{\text{in}}(\omega) \tilde{a}_j^{\text{in}\dagger}(\omega') \rangle = J_{ij}(\omega) \delta(\omega + \omega'). \quad (35)$$

We can obtain the additional noise spectrum as

$$S_{\text{add}}(\omega) = \frac{1}{2} \left\{ \gamma_m \coth\left(\frac{\hbar\omega_m}{2k_B T}\right) + |\mathcal{A}(\omega)|^2 \left[ \frac{1}{\kappa_o} + \kappa_o |\bar{\alpha}_o(\omega)|^2 + \kappa_s |\bar{\alpha}_s(\omega)|^2 + \mathcal{B}(\omega) \right] \right. \\ \left. + \omega \leftrightarrow -\omega \right\}, \quad (36)$$

where

$$\mathcal{B}(\omega) = \bar{\alpha}(\omega) \cdot \mathbf{J}(\omega) \bar{\alpha}^\dagger(-\omega) \quad (37)$$

stands for the noise induced by the non-Markovian reservoir. When  $\omega < \Delta_w - 2\xi_w$  or  $\omega > \Delta_w + 2\xi_w$  which is out of the definition of the spectrum,  $\mathcal{B}(\omega)$  will vanish, the corresponding noise is eliminated. However, the disappearance of  $\mathcal{B}(\omega)$  does not mean the lowest noise because the other noise in Eq. (36) may be amplified when  $\mathcal{B}(\omega)$  vanishes.

We now investigate the optical noise  $F_{s_o}$  which is the sensitivity  $F_s$  when we temporally ignore the thermal noise of the oscillator. In Fig. 3(a), the green curve with  $\xi_w = 12\omega_m$  corresponds to no bound state, and that with  $\xi_w = 2.4\omega_m, 3\omega_m$  correspond to the bound states. The red curve reaches to an ultrahigh sensitivity which is smaller than the zero-point fluctuation of oscillator (grey dashed line), when the bound states resonate with mechanical oscillator, i.e., around  $\omega/\omega_m = 1$ . Notice for the three values of  $\xi_w$ , the sensitivity is not monotonously affected by  $\xi_w$ . For larger value of  $\xi_w$ , there is no bound state but stronger field input, while for small  $\xi_w$ , the CROW can not efficiently transfer the information. The results corresponds to Fig. 2(a). The blue curve as well as the red one has at least two dips. The blue curve exhibits more sideband because the bound states do not resonate with the oscillator.

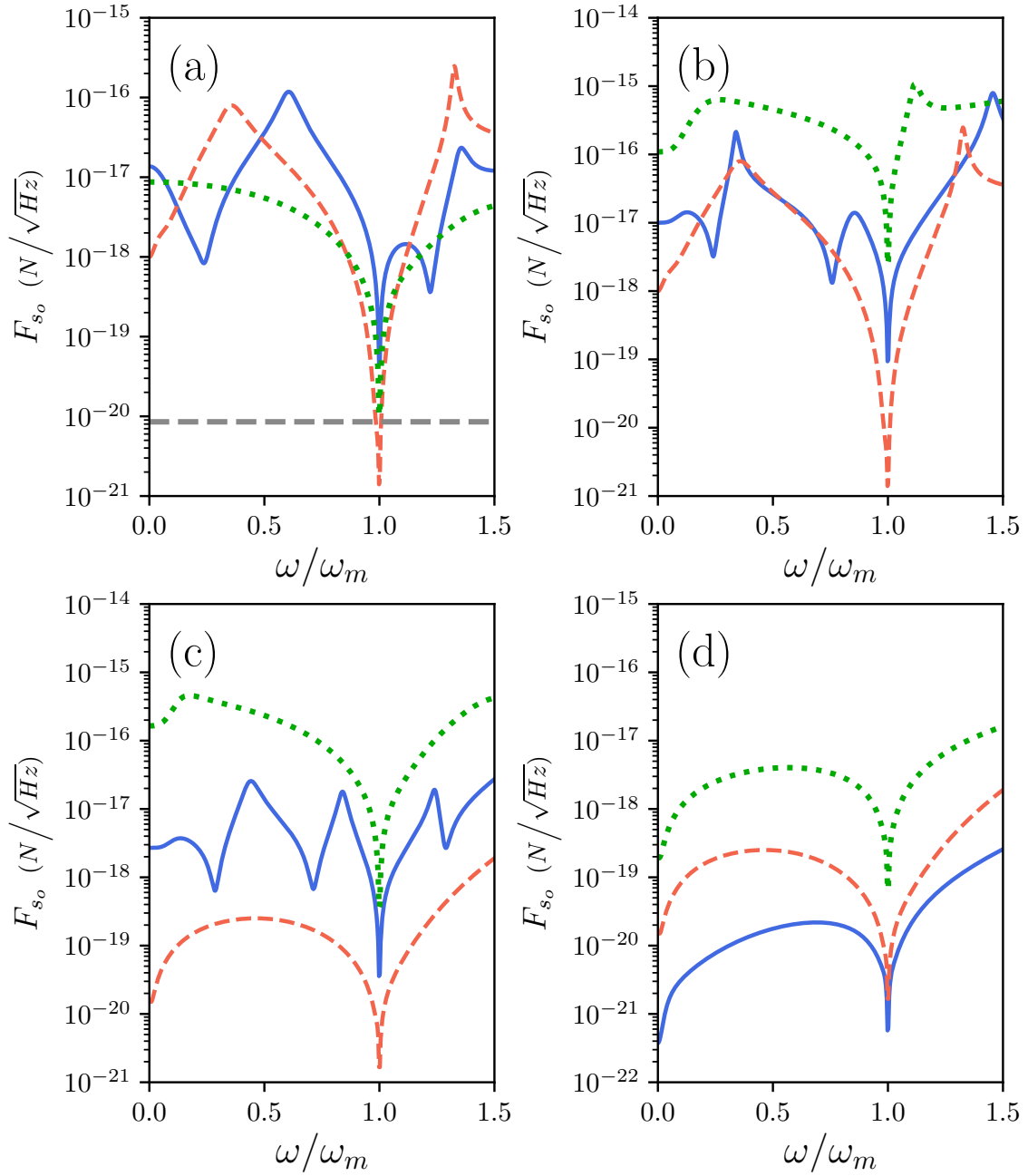


FIG. 3. The sensitivity of the sensor (the thermal noise absent) affected by several parameters where (a):  $\xi_w = 2.4\omega_m$  (blue solid),  $3\omega_m$  (red dashed) and  $12\omega_m$  (green dotted), (b):  $\xi_s = 6\omega_m$  (blue solid),  $4\omega_m$  (red dashed) and  $8\omega_m$  (green dotted), (c):  $\Delta_s = 2\omega_m$  (blue solid),  $2.4\omega_m$  (red dashed), and  $8\omega_m$  (green dotted), and (d):  $\Delta_o = 0.8\omega_m$  (blue solid),  $2\omega_m$  (red dashed), and  $6\omega_m$  (green dotted), where  $\Delta_s = 2.4\omega_m$  in (d). The grey dashed line in (a) represents the sensitivity corresponding to zero-point fluctuation noise. Here,  $\gamma_m = 10^{-5}\omega_m$ ,  $\omega_m/2\pi = 0.5\text{GHz}$ ,  $m = 1.4 \times 10^{-18}\text{kg}$  and  $\theta = \pi/2$ . Other parameters which are unspecified are same with Fig. 2.

We next study the additional noise  $F_{s_o}$  affected by  $\xi_s$ , shown in Fig. 3(b). Though a large  $\xi_s$  ensures the existence of bound state, an overlarge  $\xi_s$  will increase the effective loss of cavity field. This is because  $\xi_s$  is the coupling between the cavity  $S$  and the CROW (reservoir), meaning more photons are lost and the linearized optomechanical coupling is decreased. Therefore, the green curve is above the red one, in Fig. 3(b). For  $\xi_s = 4\omega_m$ ,  $\omega_{r_1} \approx \omega_{r_2} \approx \omega_m$  leads to the linearized cavity field  $a_s$  with the frequency  $\omega_{r_1}$  ( $\omega_{r_2}$ ). Then the cavity field will resonate to the sensing mechanical oscillator; therefore we can achieve high sensitivity, see the red curve in Fig. 3(b). When  $\xi_s = 6\omega_m$ , the high sensitivity can be reached at the sidebands, though it is worse than the red curve where the two bound states resonate with oscillator. When bound states do not resonate with oscillator, we can realize a wideband detection, though it decreases the sensitivity slightly.

In Fig. 3(c), we show the effect of the detuning  $\Delta_s$  on the sensitivity. For the green curve, a bound state vanishes and a pole corresponding to exponential decay appears, which is demonstrated in Fig. 2(c). Therefore, the sensitivity without bound state is worse than that with bound states (blue and red curves). When  $\Delta_s = 2\omega_m$  (corresponding to the blue curve in Fig. 3(c)), we can find the  $\omega_{r_1} \approx -0.29\omega_m$  (relative to the frequency of pump field  $\omega_d$ ) and  $\omega_{r_2} \approx \omega_m$  (see Fig. 2(c)). Since one of frequency of the bound states is different from  $\omega_m$ , we can observe several dips. For  $\Delta_s = 2.4\omega_m$ , we have  $\omega_{r_1} \approx 0$  and  $\omega_{r_2} \approx \omega_m$  (see Fig. 2(c)). Under this case, the red curve shows us an ultrahigh sensitivity where in wide range of frequency the sensitivity is better than that of red curve, as shown in Fig. 3(a) and (b).  $\omega_{r_1} \approx 0$  means that the bound state resonates with driven field, the classical part of the cavity is increased. When  $\omega_{r_1}$  is very close to zero,  $\alpha_s(\infty)$  is amplified greatly, and then the effective optomechanical coupling is enhanced because the effective optomechanical coupling  $G$  is proportional to  $\alpha_s(\infty)$ . Meanwhile, the other bound state with  $\omega_{r_2} \approx \omega_m$  is resonant with optomechanical oscillator. Therefore, we can achieve ultrahigh sensitivity.

In Fig. 3(d), we investigate the sensitivity with different  $\Delta_o$  where we choose  $\Delta_s = 2.4\omega_m$ . The blue curve with  $\Delta_o = 0.8\omega_m$  corresponds to  $\omega_{r_1} \approx \omega_{r_2} \approx 0$  which we have mentioned in the discussion of Fig. 2(d). In this case, although the effective optomechanical coupling can be enhanced, the sensitivity is not so good as that shown in red curve where  $\Delta_o = 2\omega_m$  leads to  $\omega_{r_1} \approx 0$  and  $\omega_{r_2} \approx \omega_m$ . For the green curve, only one bound state exists, and the sensitivity is decreased.

From Fig. 3, we conclude that we can obtain high sensitivity in three cases. The first



case is  $\omega_{r_1} \approx \omega_{r_2} \approx \omega_m$ , which realizes the sideband coupling between bound states and mechanical oscillator. However, the bound states can not be well driven, and the linearized optomechanical coupling is not effectively enhanced. The second case is  $\omega_{r_1} \approx 0$  and  $\omega_{r_2} \approx \omega_m$ , which not only the linearized optomechanical coupling is enhanced, but also the bound state can sideband couple with oscillator. The third case is  $\omega_{r_1} \approx \omega_{r_2} \approx 0$ , where two bound states resonate with driven field. The last case reach the best sensitivity, due to the extremely high driving efficiency and the absence of back-action noise.

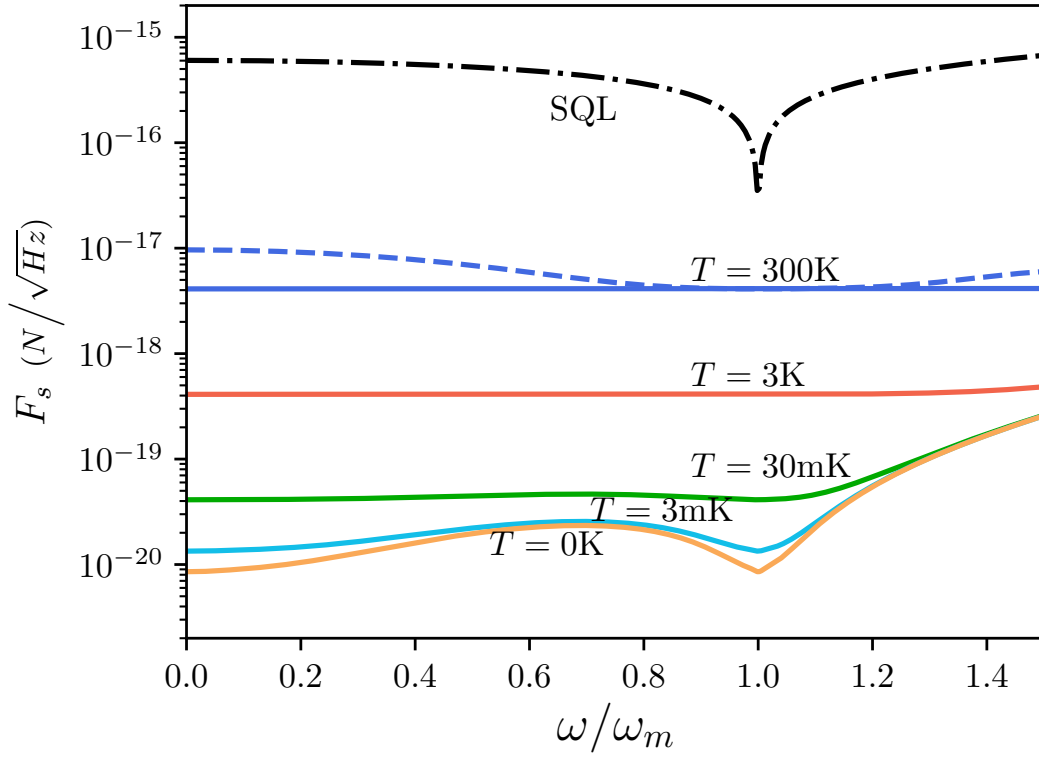


FIG. 4. The sensitivity for different temperature. The parameters are  $\Delta_w = 8\omega_m$ ,  $\xi_w = 3\omega_m$ ,  $\Delta_s = 2.4\omega_m$ ,  $\xi_s = 4\omega_m$ ,  $\Delta_o = 0.8\omega_m$ ,  $\xi_o = 2\omega_m$ , and  $\theta = \pi/2$ . The black dashdot line represents the SQL of optomechanical detection where thermal noise with  $T = 300\text{K}$  is included. The dashed curve corresponds to the green curve in Fig. 3(a). Other parameters which are unspecified are the same as in Fig. 2

Taking the thermal noise into account, we plot the total the sensitivity  $F_s$  in Fig. 4. When detect signal in room temperature, without bound state (blue dashed curve),  $F_{s_o}(\omega)$  is much larger than the thermal noise  $F_{\text{th}} \approx \sqrt{m\gamma_m k_B T} \approx 4 \times 10^{-18} \text{N}/\sqrt{\text{Hz}}$  except the

frequency around  $\omega_m$ , and the optimized  $F_{s_o}(\omega)$  in our scheme (blue solid curve) is limited by  $F_{th}$ . In weak force sensing with general optomechanical system (without back-action evasion), photon shot noise and quantum back-action leads to the so called standard quantum limit (SQL), (see [26]). As shown in Fig. 4, the level of SQL is higher than thermal noise of room temperature. With back-action evasion, we can see that the optical induced noise is almost zero because at the lowest point, the sensitivity is only limited by the thermal noise. That is to say, our proposal is better than generic optomechanical sensors even in room temperature. When  $T = 3K$ , the thermal noise dominates the sensitivity as well. We can calculate the sensitivity  $F_s \approx 4 \times 10^{-19} N/\sqrt{Hz}$ , shown in Fig. 4. When  $T = 30mK$ , the optical noise significantly impacts the additional noise, especially in the high-frequency regime. Cooling to  $3mK$  where the thermal phonon number  $n_{th} \approx 2.5$ , the sensitivity is very close to that in zero temperature.

In the optomechanical crystal regime, high quality factor of cavity and oscillator and the strong optomechanical coupling have been realized [1]. The optomechanical systems with embedded spin have also been reported [53], which may be applied to on-chip back-action-free force sensor. If pre-cooling the bath of oscillator [54], the thermal noise can be suppressed, our proposal can reach an ultrahigh sensitivity. Even in room temperature, in wide region of frequency, our proposal is better than generic optomechanical sensors, in which a higher sensitivity can be achieved under same driven field, so that the optical induced heating can be suppressed. Our scheme provide a guideline for remotely sensing quantum signal or weak force.

## V. CONCLUSION

In conclusion, we provide a proposal for high sensitivity remote weak force sensor in which the hybrid optomechanical system is back-action free through coupling to NEM oscillator. A CROW as a non-Markovian reservoir is employed for transfer the output field from the sensing cavity to the observing cavity. In order to non-dissipatively transfer the weak signals, we carefully investigate the condition of bound states. By tuning the detuning of the cavity, we can choose optimized bound states. With the assistance of bound states, an ultrahigh sensitivity with the optical noise smaller than the zero-point fluctuation, can be achieved. In frequency domain, a high sensitivity detection not only can be achieved at  $\omega \approx \omega_m$  but

also in a wide range of frequency. Even in room temperature, the optimized sensitivity with bound state is much lower than that without bound state. When the temperature is near 3mK, the sensitivity reaches  $10^{-20}N/\sqrt{Hz}$ . In our investigation, we do not included the squeezing oscillator technique and omit the loss of CROW. If we introduce the squeezing technique and take account of the loss of the CROW, the noise of CROW may be canceled by the suppressed noise with squeezing technique.

## VI. ACKNOWLEDGEMENT

This work was supported by NSFC under Grant No. 11874099 and 11674120.

### Appendix A: Green's function and bound state

In this section, we study the Green's function of the cavity field, and the position of the poles of the Green's function.

The cavity field  $\alpha_j(t)$  ( $j = s, o$ ) can be calculated through

$$\alpha_j(t) = E_o \int_0^t d\tau \bar{\alpha}_j(\tau) \quad (\text{A1})$$

where the  $\bar{\alpha}_j(\tau)$  is the corresponding Green's function. The Green's function  $\bar{\alpha}_j$  obeys Dyson equation

$$\bar{\alpha}(t) = -i\tilde{\Delta}\bar{\alpha} - \int_0^t d\tau \int d\omega \mathbf{J}(\omega)\bar{\alpha}(\tau)e^{-i\omega(t-\tau)} \quad (\text{A2})$$

where  $\bar{\alpha}(t) = [\bar{\alpha}_s(t), \bar{\alpha}_o(t)]^T$ . With the Laplace transform, we can obtain

$$\bar{\alpha}_s(z) = i \frac{\sigma_{so}(z)}{\mathcal{D}(z)}, \quad (\text{A3})$$

$$\bar{\alpha}_o(z) = i \frac{z - \tilde{\Delta}_s - \sigma_{ss}(z)}{\mathcal{D}(z)}, \quad (\text{A4})$$

where

$$\mathcal{D}(z) = [z - \tilde{\Delta}_s - \sigma_{ss}(z)][z - \tilde{\Delta}_o - \sigma_{oo}(z)] - \sigma_{so}(z)\sigma_{os}(z). \quad (\text{A5})$$

The  $\bar{\alpha}(t)$  can be solved through an inverse Laplace transformation

$$O(t) = \int_{i\lambda-\infty}^{i\lambda+\infty} \frac{dz}{2\pi} e^{-izt} O(z). \quad (\text{A6})$$

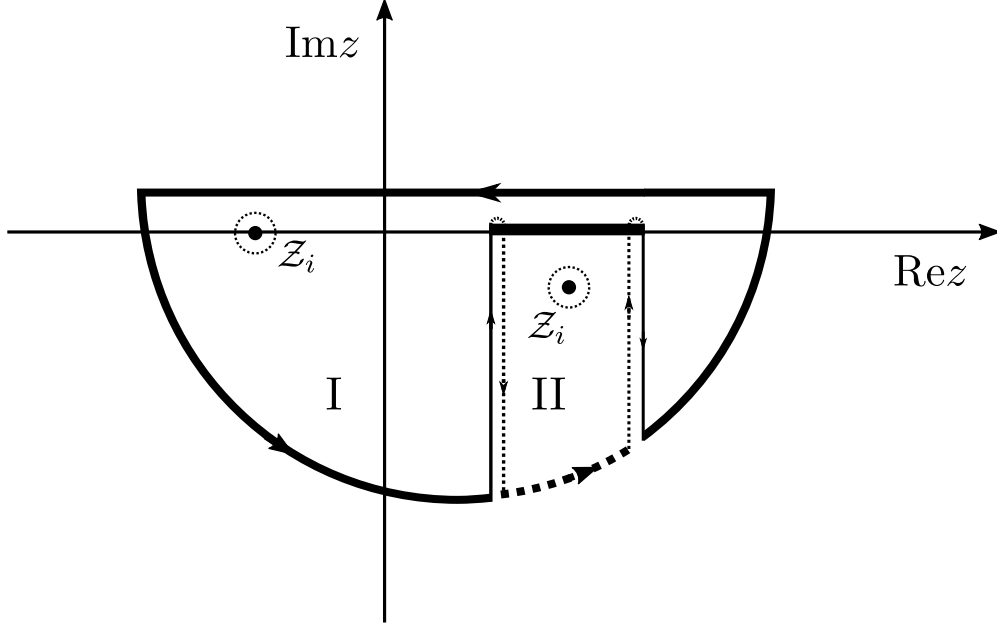


FIG. 5. The Bromwich path for inverse Laplace transformation

The integral on complex plane should be calculated through contour integral technique around the Bromwich path which is presented in Fig.5. For our system,  $\bar{\alpha}(t)$  is not analytic on complex plane where  $\Delta_w - 2\xi_w < z < \Delta_w + 2\xi_w$  is the branch cut. The contour path crosses the branch cut at  $\Delta_w - 2\xi_w$  from the first Riemannian sheet I to the second Riemannian sheet II and back from II to I at  $\Delta_w + 2\xi_w$  for guaranteeing that the integrand is analytic. On the second Riemannian sheet we define the analytic continuation of  $\sigma_{ij}(z)$  as the previous papers pointed [36].

For a CROW non-Markovian model, the poles on the first Riemannian sheet are located on real axis [36]. These poles have real part but without imaginary part that presents the dissipation or gain, which correspond to the bound states. The nature of bound state is that the modes corresponded the poles on the first Riemannian sheet can not exponentially leak to the reservoir in which the frequencies of poles are out of the cut-off frequency. Because the CROW both couple to cavity  $O$  and  $S$  in our proposal, the solution of Eq. (A5) is very complicated, and we can not analytically solve it. The mechanism of bound states is same, that is the mode with poles on first Riemannian sheet is prevented from exponentially leaking to the reservoir. The poles on first Riemannian sheet should be on the real axis in our proposal. The numerical solution supports that deduction as well. There is another sort of poles located on the second Riemannian sheet. These poles stand for exponential decay with

an effective decay rate and effective frequency shift, which can be easily obtained after the Weisskopf-Wigner approximation in open quantum system regime. When the environment spectrum tends to an infinity flat spectrum that is to say a typical Markovian condition, the poles on the second Riemannian sheet corresponds to the exponential decay of system.

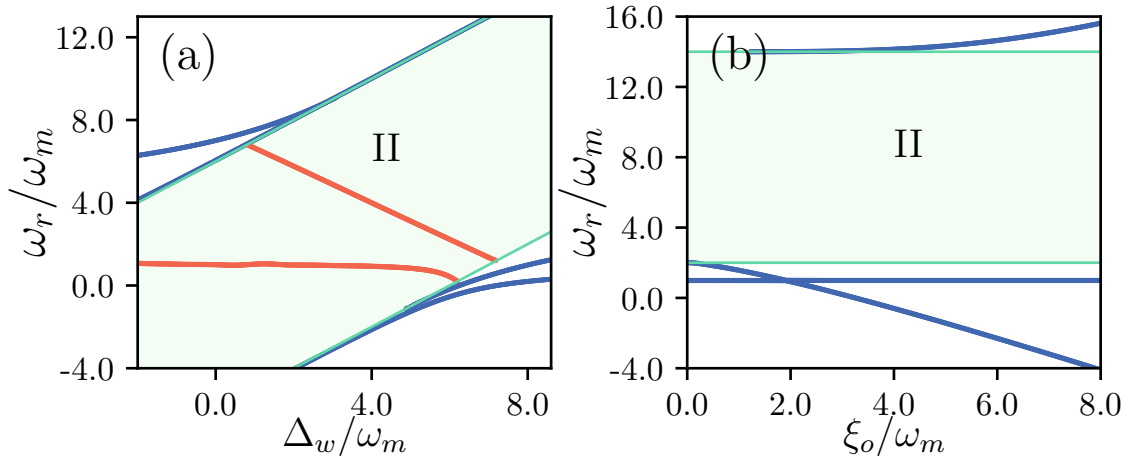


FIG. 6. The frequency  $\omega_r$  as the function of  $\Delta_w$  (a) and  $\xi_o$  (b). Other parameters are same with Fig. 2

We have discussed the  $\omega_r$  as the function of  $\xi_w$ ,  $\xi_s$ ,  $\Delta_s$  and  $\Delta_o$ , in main body. As shown in Fig. 6(a), the bound state only exist when the frequency of cavity  $S$  and  $O$  significantly mismatches the frequency of the cavity of CROW. When  $\Delta_w > 6\omega_m$ , there are two bound states, and the difference of their frequency increases with  $\Delta_w$ . With the changing of  $\Delta_w$ , the exponential decay will disappear suddenly, while the bound states continually change. As shown in Fig. 6(b), all the poles are on the first Riemannian sheet. For the CROW system, when  $|\Delta_w - \Delta_o| \gg \xi_w$ , it is strong non-Markovian, where the bound states will be generated [36].

## Appendix B: Long-time solution of classical mean value

With the inverse Laplace transform of Eq. (A3) and contour integral technique, we obtain

$$\bar{\alpha}_s(t) = \sum_n \mathcal{Z}_n e^{-i\omega_{rn}} + \left( \int_{\omega_1 - i\infty}^{\omega_1} - \int_{\omega_2 - i\infty}^{\omega_2} \right) \frac{dz}{2\pi} e^{-izt} [\bar{\alpha}_s^{\text{II}}(z) - \bar{\alpha}_s^{\text{I}}(z)], \quad (\text{B1})$$

where  $\mathcal{Z}_n$  is the residues of  $\bar{\alpha}_s(z)$  corresponding to the pole at  $z = \omega_{r_n}$  on the first and the second Riemannian sheet, and the last term describes the non-exponential decay.

According to Eqs. (B1) and (A1), we can obtain  $\alpha_s(t)$ . Especially, we focus on the long-time limit  $\alpha_s(t \rightarrow \infty)$  which plays a key role in our proposal. The fast decay term of  $\alpha_s(t)$  are negligible, thus we can obtain

$$\alpha_s(t \rightarrow \infty) = \sum_{n'} \frac{iE}{\omega_{r_{n'}}} \mathcal{Z}_{n'} e^{-i\omega_{r_{n'}} t} - iE \sum_n \frac{\mathcal{Z}_n}{\omega_{r_n}} + I_{\text{NE}},$$

where only the poles corresponding to bound state contribute to the first term with notation  $n'$ , the second term takes all the poles into consideration with notation  $n$ , and the last term

$$I_{\text{NE}} = E_s \int_0^t d\tau \left( \int_{\omega_1 - i\infty}^{\omega_1} - \int_{\omega_2 - i\infty}^{\omega_2} \right) \frac{dz}{2\pi} e^{-iz\tau} [\bar{\alpha}_s^{\text{I}}(z) - \bar{\alpha}_s^{\text{II}}(z)], \quad (\text{B2})$$

is contributed by the non-exponential decay.

The bound states may exist or not. If no bound states  $G = \alpha_s g$  is time-independent, otherwise  $G = G_0 + \sum_j G_{r_j} e^{-\omega_{r_j} t}$ .

### Appendix C: non-exponential decay

In the non-Markovian system, the non-exponential decay appears frequently, which results from the violation of Weisskopf-Wigner approximation. Here, it reflects in the second term of Eq. (B1) which is the integral through vertical path, as shown in Fig. 5:

$$\bar{I}_1(t) = \int_{\omega_1 - i\infty}^{\omega_1} \frac{dz}{2\pi} e^{-izt} [\bar{\alpha}_s^{\text{I}}(z) - \bar{\alpha}_s^{\text{II}}(z)], \quad (\text{C1})$$

with the transformation  $x = i(z - \omega_1)$ , we obtain

$$\bar{I}_1(t) = \frac{ie^{-i\omega_1 t}}{2\pi} \int_0^\infty dx e^{-xt} [\bar{\alpha}_s^{\text{I}}(\omega_1 - ix) - \bar{\alpha}_s^{\text{II}}(\omega_1 - ix)], \quad (\text{C2})$$

The third term of Eq. (B1) can be obtained by similar operation as

$$\bar{I}_2(t) = -\frac{ie^{-i\omega_2 t}}{2\pi} \int_0^\infty dx e^{-xt} [\bar{\alpha}_s^{\text{I}}(\omega_2 - ix) - \bar{\alpha}_s^{\text{II}}(\omega_2 - ix)]. \quad (\text{C3})$$

In general,  $\bar{I}_1(t)$  and  $\bar{I}_2(t)$  indicate the non-exponential decay in non-Markovian dynamic. As the Eqs. (C2) and (C3) indicating, the two integrals are convergent. The influence of non-exponential decay can be taken into consideration through numerical calculating the  $\bar{I}_1(t)$

and  $\bar{I}_2(t)$ . In general, the non-exponential decay can decrease the loss of photon number of sensing cavity, comparing the exponential decay.

- 
- [1] M. Aspelmeyer, T. J. Kippenberg, and F. Marquardt, *Rev. Mod. Phys.* **86**, 1391 (2014).
  - [2] Y. Chen, *J. Phys. B At. Mol. Opt. Phys.* **46**, 104001 (2013).
  - [3] M. Cai, O. Painter, and K. J. Vahala, *Phys. Rev. Lett.* **85**, 74 (2000).
  - [4] M. Tomes and T. Carmon, *Phys. Rev. Lett.* **102**, 113601 (2009).
  - [5] H. Lü, C. Wang, L. Yang, and H. Jing, *Phys. Rev. Applied* **10**, 014006 (2018).
  - [6] A. Schliesser, O. Arcizet, R. Rivière, G. Anetsberger, and T. J. Kippenberg, *Nat. Phys.* **5**, 509 (2009).
  - [7] Z. Shen, Y.-L. Zhang, Y. Chen, C.-L. Zou, Y.-F. Xiao, X.-B. Zou, F.-W. Sun, G.-C. Guo, and C.-H. Dong, *Nat. Photonics* **10**, 657 (2016).
  - [8] R. Reimann, M. Doderer, E. Hebestreit, R. Diehl, M. Frimmer, D. Windey, F. Tebbenjohanns, and L. Novotny, *Phys. Rev. Lett.* **121**, 033602 (2018).
  - [9] T. M. Hoang, Y. Ma, J. Ahn, J. Bang, F. Robicheaux, Z.-Q. Yin, and T. Li, *Phys. Rev. Lett.* **117**, 123604 (2016).
  - [10] M. Eichenfield, J. Chan, R. M. Camacho, K. J. Vahala, and O. Painter, *Nature* **462**, 78 (2009).
  - [11] J. Bochmann, A. Vainsencher, D. D. Awschalom, and A. N. Cleland, *Nat. Phys.* **9**, 712 (2013).
  - [12] E. Gavartin, P. Verlot, and T. J. Kippenberg, *Nat. Nanotechnol.* **7**, 509 (2012).
  - [13] C. Doolin, P. H. Kim, B. D. Hauer, A. J. R. MacDonald, and J. P. Davis, *New J. Phys.* **16**, 035001 (2014).
  - [14] G. Anetsberger, O. Arcizet, Q. P. Unterreithmeier, R. Rivière, A. Schliesser, E. M. Weig, J. P. Kotthaus, and T. J. Kippenberg, *Nat. Phys.* **5**, 909 (2009).
  - [15] M. Erdil, Y. Ozer, and S. Kocaman, *IEEE Journal of Selected Topics in Quantum Electronics* **25**, 1 (2019).
  - [16] J. Arlett, E. Myers, and M. Roukes, *Nat. Nanotechnol.* **6**, 203 (2011).
  - [17] X.-y. Lü, Y. Wu, J. R. Johansson, H. Jing, J. Zhang, and F. Nori, *Phys. Rev. Lett.* **114**, 093602 (2015).

- [18] C. U. Lei, A. J. Weinstein, J. Suh, E. E. Wollman, A. Kronwald, F. Marquardt, A. A. Clerk, and K. C. Schwab, *Phys. Rev. Lett.* **117**, 100801 (2016), arXiv:1605.08148.
- [19] X. Wang, H.-r. Li, P.-b. Li, C.-w. Jiang, H. Gao, and F.-l. Li, *Phys. Rev. A* **90**, 013838 (2014).
- [20] R. Zhang, Y. Fang, Y.-Y. Wang, S. Chesil, and Y.-D. Wang, *Phys. Rev. A* **99**, 043805 (2019).
- [21] R. S. Bondurant and J. H. Shapiro, *Phys. Rev. D* **30**, 2548 (1984).
- [22] Z. Wen, Z. Sheng-Dian, M. Adam, and J. Hui, *Sci. China-Phys. Mech. Astron.* **63**, 224211 (2020).
- [23] Y. Ma, S. L. Danilishin, C. Zhao, H. Miao, W. Z. Korth, Y. Chen, R. L. Ward, and D. G. Blair, *Phys. Rev. Lett.* **113**, 151102 (2014).
- [24] T. Briant, M. Cerdonio, L. Conti, A. Heidmann, A. Lobo, and M. Pinard, *Phys. Rev. D* **67**, 102005 (2003).
- [25] M. J. Woolley and A. A. Clerk, *Phys. Rev. A* **87**, 063846 (2013).
- [26] A. Motazedifard, F. Bemani, M. H. Naderi, R. Roknizadeh, and D. Vitali, *New J. Phys.* **18**, 073040 (2016).
- [27] F. Bariani, H. Seok, S. Singh, M. Vengalattore, and P. Meystre, *Phys. Rev. A* **92**, 043817 (2015).
- [28] G. Tesfay, Z. Ye-Xiong, M. Mojtaba, and L. Chong, *Sci. China-Phys. Mech. Astron.* **63**, 210311 (2020).
- [29] M. Tsang and C. M. Caves, *Phys. Rev. Lett.* **105**, 123601 (2010).
- [30] K. Zhang, P. Meystre, and W. Zhang, *Phys. Rev. A* **88**, 043632 (2013).
- [31] C. B. Mller, R. A. Thomas, G. Vasilakis, E. Zeuthen, Y. Tsaturyan, M. Balabas, K. Jensen, A. Schliesser, K. Hammerer, and E. S. Polzik, *Nature* **547**, 191 (2017).
- [32] W. Chen, S. Kaya Özdemir, G. Zhao, J. Wiersig, and L. Yang, *Nature* **548**, 192 (2017).
- [33] S. Liu, W. Sun, Y. Wang, X. Yu, K. Xu, Y. Huang, S. Xiao, and Q. Song, *Optica* **5**, 612 (2018).
- [34] S. Wang, J. Lin, Y. Huang, Y. Yang, K. Che, J. Xiao, Y. Du, and Z. Fan, *IEEE Photonics Technology Letters* **22**, 1349 (2010).
- [35] I. de Vega and D. Alonso, *Rev. Mod. Phys.* **89**, 015001 (2017).
- [36] S. Longhi, *Phys. Rev. A* **74**, 063826 (2006).
- [37] P. Lodahl, S. Mahmoodian, and S. Stobbe, *Rev. Mod. Phys.* **87**, 347 (2015).



- [38] J.-Q. Liao, Z. R. Gong, L. Zhou, Y.-x. Liu, C. P. Sun, and F. Nori, *Phys. Rev. A* **81**, 042304 (2010).
- [39] X.-W. Xu, A.-X. Chen, Y. Li, and Y.-x. Liu, *Phys. Rev. A* **95**, 063808 (2017).
- [40] U. Hoeppe, C. Wolff, J. Küchenmeister, J. Niegemann, M. Drescher, H. Benner, and K. Busch, *Phys. Rev. Lett.* **108**, 043603 (2012).
- [41] H.-T. Tan, W.-M. Zhang, and G.-x. Li, *Phys. Rev. A* **83**, 062310 (2011).
- [42] F. Ciccarello, *Phys. Rev. A* **91**, 062121 (2015).
- [43] C. Gonzalez-Ballester, F. J. García-Vidal, and E. Moreno, *New J. Phys.* **15**, 073015 (2013).
- [44] H. Z. Shen, S. Xu, H. T. Cui, and X. X. Yi, *Phys. Rev. A* **99**, 032101 (2019).
- [45] W.-M. Zhang, P.-Y. Lo, H.-N. Xiong, M. W.-Y. Tu, and F. Nori, *Phys. Rev. Lett.* **109**, 170402 (2012).
- [46] T. Quang, M. Woldeyohannes, S. John, and G. S. Agarwal, *Phys. Rev. Lett.* **79**, 5238 (1997).
- [47] C. W. Hsu, B. Zhen, A. D. Stone, J. D. Joannopoulos, and M. Soljačić, *Nat. Rev. Mater.* **1**, 16048 (2016).
- [48] W.-Z. Zhang, Y. Han, B. Xiong, and L. Zhou, *New J. Phys.* **19**, 083022 (2017).
- [49] J. Kohler, J. A. Gerber, E. Dowd, and D. M. Stamper-Kurn, *Phys. Rev. Lett.* **120**, 013601 (2018).
- [50] L. Zhou, J. Cheng, Y. Han, and W. Zhang, *Phys. Rev. A* **88**, 063854 (2013).
- [51] G. Ranjit, D. P. Atherton, J. H. Stutz, M. Cunningham, and A. A. Geraci, *Phys. Rev. A* **91**, 051805(R) (2015).
- [52] V. Giovannetti and D. Vitali, *Phys. Rev. A* **63**, 023812 (2001).
- [53] J. V. Cady, O. Michel, K. W. Lee, R. N. Patel, C. J. Sarabalis, A. H. Safavi-Naeini, and A. C. B. Jayich, *Quantum Science and Technology* **4**, 024009 (2019).
- [54] J. Chan, T. P. M. Alegre, A. H. Safavi-Naeini, J. T. Hill, A. Krause, S. Gröblacher, M. Aspelmeyer, and O. Painter, *Nature* **478**, 89 (2011).